

First-principles investigation of the alloy scattering potential in dilute Si_{1-x}C_xM. P. Vaughan,^{1,*} F. Murphy-Armando,¹ and S. Fahy^{1,2}¹*Tyndall National Institute, Lee Maltings, Cork, Ireland*²*Department of Physics, University College Cork, Cork, Ireland*

(Received 24 November 2011; revised manuscript received 11 April 2012; published 23 April 2012)

A first-principles method is applied to find the intra and intervalley n -type carrier scattering rates for substitutional carbon in silicon. The method builds on a previously developed first-principles approach with the introduction of an interpolation technique to determine the intravalley scattering rates. Intravalley scattering is found to be the dominant alloy scattering process in Si_{1-x}C_x, followed by g -type intervalley scattering. Mobility calculations show that alloy scattering due to substitutional C alone cannot account for the experimentally observed degradation of the mobility. We show that the incorporation of additional charged impurity scattering due to electrically active interstitial C complexes models this residual resistivity well.

DOI: [10.1103/PhysRevB.85.165209](https://doi.org/10.1103/PhysRevB.85.165209)

PACS number(s): 72.20.Dp, 72.20.Fr, 72.80.Cw

I. INTRODUCTION

The introduction of carbon into SiGe/Ge heterostructures is of technological interest due to the dual effects of strain compensation in the Si_{1-y}Ge_y layers¹ and suppression of the out-diffusion of p -type acceptors, in particular, boron² and indium,³ during wafer fabrication. The transport properties of the material are expected to be modified by two competing processes. On the one hand, in silicon, the induced strain will lift the degeneracy of the Δ valleys allowing the conduction electrons to see a smaller effective mass for transport in the appropriate direction and reducing intervalley scattering. On the other hand, the substitutional carbon is likely to introduce alloy scattering, acting to reduce the mobility.

Transport measurements by Osten *et al.*⁴ of tensile strained Si_{1-x}C_x and compressive strained Si_{1-y-x}Ge_yC_x show a degradation of the n - and p -type Hall mobility, respectively, as the carbon concentration is increased. This is in contrast to the earlier measurements of Eberl *et al.*,⁵ who reported an improvement of the mobility with C doping. However, Osten *et al.* reported that their findings showed evidence of the formation of electrically active defects due to interstitial carbon complexes. This is consistent with the identification of both donor⁶ and acceptor states⁷ due to interstitial carbon in silicon, C_i (a C and Si atom sharing the same lattice site). Additionally, the C_iC_s complex (a C interstitial bonded to a substitutional C atom) has been found to exist in positive, negative, and neutral charge states.^{8,9}

Such electrically active states would introduce strong ionized impurity scattering at low temperatures in addition to any deliberate doping, whilst neutral impurity scattering would be expected to lower the mobility over all temperatures. It is important, then, to disentangle the contributions of interstitial and substitutional carbon.

In the current work, we investigate electron scattering due to substitutional carbon via a first-principles approach developed by Murphy-Armando and Fahy.^{10,11} The aims of this work are threefold: (1) given the large difference in covalent radii and electronegativity between C and Si, we might speculate that C would produce a localized state, resonant with the conduction band in analogy to nitrogen in III-V materials such as GaInAs.¹² If this proved to be the case, we might expect very strong alloy scattering much as we do in the

dilute nitrides.¹³ Moreover, the method for calculating the alloy scattering parameters developed in Refs. 10 and 11 and extended in the current work would not be directly applicable to such a resonant state.

(2) The validity of our method for calculating the alloy scattering matrix has already been demonstrated for elemental alloys in Refs. 10,11. In this paper, we extend the method by introducing a \mathbf{q} -point interpolation scheme to overcome the problem of the arbitrary zero of the potential (discussed in detail in Sec. III D) and better facilitate the calculation of intravalley scattering. We can then directly compare the methods for the calculation of g -type scattering (see Sec. II) to ensure consistency.

(3) The transport measurements for Si_{1-x}C_x by Osten *et al.*⁴ show a severe degradation of the mobility with C doping, showing the imposition of a limiting mobility with a temperature dependence characteristic of scattering from ionized impurities. This is believed to be due to electrically active C interstitials. Since we are able to calculate the scattering rate for substitutional carbon (rather than take this as a fitting parameter as is usually done for alloy scattering), we are able to fit the residual mobility using a model of ionized impurity scattering and thereby obtain estimates of the unknown electrically active interstitial concentrations.

Note that we do not attempt to apply the first-principles method of impurity scattering to the C interstitials for two reasons. Firstly, a first-principles study of all possible C interstitials would constitute a major piece of work in itself that has already been pursued by other authors. However, since we would need the full output files for these computations, we would still need to reproduce this. Secondly, the method we use would only be applicable to neutral impurity scattering from the non-ionized dopants. This would only be significant at very low temperatures where carrier freeze out pertains. At higher temperatures, the scattering from these impurities would be dominated by the Coulomb interaction for which very good models already exist. The original motivation for investigating alloy scattering via a first-principles approach is that models based on a physical understanding of the scattering potential do not exist and it is the magnitude of the matrix element that is usually taken as a fitting parameter.

In the next section, we discuss electronic transport in biaxially strained Si, presenting expressions for the drift mobility in non-degenerate, parabolic bands. The formal model of alloy scattering is then presented, introducing the scattering matrix elements that we wish to calculate using the first-principles techniques described in Sec. III. In Sec. IV, we use our results to calculate the alloy scattering-limited mobility and compare this to the experimental data.

II. MOBILITY IN BIAXIALY STRAINED SI(1-X)C(X)

A. General expressions

In silicon, low-electric field electron transport occurs in the six equivalent spheroidal valleys along each Δ line in the Brillouin zone. In the following discussion, we shall treat the energy dispersion as parabolic in both the longitudinal (major axis of spheroid) and transverse (minor axis) directions. The valleys are then characterized by the longitudinal and transverse effective masses, m_l and m_t , respectively.

The transport properties are calculated via the low-electric field solution of the Boltzmann transport equation (BTE). For purely elastic scattering processes, this yields a momentum relaxation time $\tau_{n,\mathbf{k}}$ for a state with band index n , wave vector \mathbf{k} , and energy $\epsilon_{n,\mathbf{k}}$ given by

$$\frac{1}{\tau_{n,\mathbf{k}}} = \sum_{n'} \int s_{\mathbf{k}\mathbf{k}'}^{n'n} (1 - \cos \alpha') \frac{V_C}{(2\pi)^3} d^3\mathbf{k}' \equiv W(\epsilon_{n,\mathbf{k}}), \quad (1)$$

where α' is the angle between \mathbf{k} and \mathbf{k}' , V_C is the crystal volume, and $W(\epsilon_{\mathbf{k}})$ is the energy dependent scattering rate. From time-dependent perturbation theory, we have

$$s_{\mathbf{k}\mathbf{k}'}^{n'n} = \frac{2\pi}{\hbar} |M_{\mathbf{k}\mathbf{k}'}^{nn'}|^2 \delta(\epsilon_{\mathbf{k}'} - \epsilon_{\mathbf{k}}), \quad (2)$$

where $M_{\mathbf{k}\mathbf{k}'}^{nn'}$ is the matrix element for scattering from electron state labeled by (n, \mathbf{k}) to state (n', \mathbf{k}') . Note that, in general, $M_{\mathbf{k}\mathbf{k}'}^{nn'}$ will be a sum of matrix elements for all elastic processes. Moreover, we may also find an effective $\tau_{n,\mathbf{k}}$ including inelastic processes via solution of the BTE, although not usually in such a simple form (see, for instance Ref. 14).

We now restrict our consideration to scattering within and between the Δ valleys. Dropping the band index notation, the scattering rate in a particular valley labeled by α may be written as a sum of different scattering processes:

$$W_\alpha(\epsilon) = \sum_i W_i(\epsilon). \quad (3)$$

The processes summed over in Eq. (3) are classified into three types: intravalley, f -type intervalley, and g -type intervalley scatterings. f -type scattering occurs from a valley lying along one Δ line to one of the other four valleys lying in an orthogonal direction, whereas in g -type scattering, the scattering is into the valley diametrically opposite the initial valley along the same Cartesian direction.

Since the lattice constant of $\text{Si}_{1-x}\text{C}_x$ is less than that of silicon, $\text{Si}_{1-x}\text{C}_x$ grown on an Si substrate is subject to a biaxial tensile strain. This leads to a splitting of the six degenerate Δ valleys. The two valleys along axes parallel to the growth direction (the out-of-plane direction) are lowered in energy (referred to as “lower” valleys), whilst the other

four orthogonal valleys (parallel to the in-plane direction) are raised (“upper valleys”). We shall denote the energy splitting between the upper and lower valleys by $\Delta\epsilon$.

In the absence of biaxial strain, the mobility is the same in all directions, with the conduction electrons seeing a combined effective mass of $3(1/m_l + 2/m_t)^{-1}$. As $\Delta\epsilon/k_B T \rightarrow \infty$, where k_B is Boltzmann’s constant and T is the absolute temperature, the in-plane conduction electrons see only the transverse effective mass m_t . Conversely, the out-of-plane conduction electrons see only m_l . Since $m_l > m_t$, if all other factors remained equal, we would expect to see an enhancement of the in-plane mobility and a degradation of the out-of-plane mobility relative to unstrained Si.

Additionally, at low temperatures, we would also expect to see a suppression of intervalley scattering into the upper valleys. Hence the scattering originating in either of the two lower valleys at low temperatures may only be intravalley or g -type intervalley. This mobility enhancement will be in competition with any degradation due to alloy scattering or any other process induced by the introduction of C into Si.

For non-degenerate, parabolic bands, the in-plane and out-of-plane drift mobilities μ_{in} and μ_{out} are found to be

$$\mu_{\text{in}}(T) = \frac{e}{m_t} \frac{\langle \tau_1 \rangle (1 + m_l/m_t) e^{-\Delta\epsilon/k_B T} + \langle \tau_0 \rangle}{(2e^{-\Delta\epsilon/k_B T} + 1)} \quad (4)$$

and

$$\mu_{\text{out}}(T) = \frac{e}{m_l} \frac{2\langle \tau_1 \rangle (m_l/m_t) e^{-\Delta\epsilon/k_B T} + \langle \tau_0 \rangle}{(2e^{-\Delta\epsilon/k_B T} + 1)}, \quad (5)$$

where

$$\langle \tau_\alpha \rangle = \frac{\int_0^\infty \tau_\alpha(\epsilon) e^{-\epsilon/k_B T} \epsilon^{3/2} d\epsilon}{\int_0^\infty e^{-\epsilon/k_B T} \epsilon^{3/2} d\epsilon}. \quad (6)$$

The indices 1 and 0 label the higher and lower valleys, respectively, and $\tau_\alpha(\epsilon) = 1/W_\alpha(\epsilon)$ is the relaxation time. Note that, in general, the energy-dependent relaxation times will also be temperature dependent (for example, when an effective relaxation time is used including phonon scattering). $\langle \tau_\alpha \rangle$ represents an energy averaging of the relaxation time, requiring a factor of $\epsilon D(\epsilon)$, where $D(\epsilon)$ is the density of states, in the integrals. In the parabolic case, this is proportional to $\epsilon^{3/2}$.

Equations (4) to (6) are the expressions that we solve numerically to determine the mobility. Note that in these expressions, the scattering rate should be expanded in terms of the rates for intravalley, f -type, and g -type scatterings, denoted by $W_\Delta(\epsilon)$, $W_f(\epsilon)$, and $W_g(\epsilon)$, respectively, according to

$$W_0(\epsilon) = W_\Delta(\epsilon) + W_g(\epsilon) + 4W_f(\epsilon - \Delta\epsilon) \quad (7)$$

and

$$W_1(\epsilon) = W_\Delta(\epsilon) + W_g(\epsilon) + 2[W_f(\epsilon) + W_f(\epsilon + \Delta\epsilon)]. \quad (8)$$

B. The alloy scattering rate

The model of alloy scattering developed by Flinn,¹⁵ based on the virtual crystal approximation (VCA) due to Nordheim,¹⁶

and later by Asch and Hall^{17,18} for binary metallic alloys suffices as the formal framework for the current work based on the first-principles approach. The first-principles approach takes as its starting point the construction of supercells modeling a perturbed system for which we find the ground-state density and, subsequently, the Hamiltonian of the system via the supercell eigenvalues and eigenstates, as described in detail in the next section. For the formal model of alloy scattering, we simply reinterpret the number of ions in the sample N as the number of atoms in a supercell and V_C as the supercell volume. (Note that the alloy scattering rate introduced by Harrison and Hauser for ternary III-V semiconductor alloys¹⁹ is based on the more fundamental work of Flinn, Asch, and Hall but with the incorporation of specific modeling simplifications not imposed here).

The alloy scattering model assumes that the potential can be decomposed into two parts: the VCA potential, being an average potential weighted according to the proportions of each species, and a random part due to the difference in potential $\Delta V(\mathbf{r})$ arising from the substitution of one atomic species for the other. It is this random part that provides a perturbation giving rise to scattering. Hereafter, we refer to $\Delta V(\mathbf{r})$ as the alloy scattering potential.

Following through the analysis in the above references, we find that the squared modulus of the alloy scattering matrix element for the transition of a state $|\alpha\rangle$ to a state $|\beta\rangle$ in a completely random alloy is given by

$$|M_{\alpha\beta}|^2 = \frac{x(1-x)}{N} |\langle V_{\alpha\beta} \rangle|^2, \quad (9)$$

where we have defined

$$\langle V_{\alpha\beta} \rangle = N \langle \beta | \Delta V_{AB}(\mathbf{r}) | \alpha \rangle. \quad (10)$$

The calculation of the quantity $\langle V_{\alpha\beta} \rangle$ will be the principal task of the present work.

In the case that the scattering matrix element is isotropic, Eq. (1) reduces to Fermi's golden rule, with the indices α and β now taken to label valleys. The alloy scattering rate may then be written down as

$$\frac{1}{\tau_\alpha(\epsilon)} = x(1-x) \frac{(2m_d^*)^{3/2} a_0^3}{16\pi\hbar^4} \sum_\beta |\langle V_{\alpha\beta} \rangle|^2 (\epsilon - \epsilon_\beta)^{1/2}. \quad (11)$$

Here, m_d is the density of states effective mass defined by $m_d^{*3} = m_l^* m_t^{*2}$, ϵ_β is the band-edge energy of the β th valley and we have made the substitution $V_C/N = a_0^3/8$ for Si (eight atoms per cubic cell with lattice constant a_0).

Neglecting the suppression of f -type scattering at low temperatures, we may use Eq. (11) to find an approximate analytical expression for the alloy scattering-limited mobility

$$\begin{aligned} \mu_{\text{al}}(T) &= \frac{e[(1 + m_t/m_l)e^{-\Delta\epsilon/k_B T} + 1]}{m_t(2e^{-\Delta\epsilon/k_B T} + 1)} \\ &\quad \times \frac{64\pi^{1/2}\hbar^4}{3x(1-x)(2m_d^*)^{3/2}a_0^3 \sum_\beta |\langle V_{\alpha\beta} \rangle|^2 (k_B T)^{1/2}}. \end{aligned} \quad (12)$$

C. Charged impurity scattering

The observed mobilities for $\text{Si}_{1-x}\text{C}_x$ offer evidence of additional charged impurity scattering at low temperatures due to electrically active carbon interstitial complexes. This may be modeled by the Brooks-Herring formula for ionized impurity scattering,²⁰ derived using Eq. (1) with the matrix element for electron scattering from a screened Coulomb potential. The scattering rate is given by

$$W_{II}(\epsilon) = \frac{N_I Z^2 e^4}{16\pi \epsilon^2 (2m_d^*)^{1/2} \epsilon^{3/2}} S(\epsilon, T), \quad (13)$$

where N_I is the density of ionized impurities, Z is the ionization number, ϵ is the permittivity in the material, and $S(\epsilon, T)$ is a screening factor given by

$$S(\epsilon, T) = \ln[\lambda(\epsilon, T) + 1] - \frac{\lambda(\epsilon, T)}{\lambda(\epsilon, T) + 1} \quad (14)$$

and

$$\lambda(\epsilon, T) = \frac{8m_d^* \epsilon}{\hbar^2 q_0^2(T)}. \quad (15)$$

q_0 models the effect of an exponential decay imposed onto the Coulomb potential and is given by¹⁴

$$q_0^2(T) = \frac{e^2 n_e}{\epsilon k_B T}, \quad (16)$$

where n_e is the electron density. We shall assume that $Z = 1$ and that the material is uncompensated, so that $n_e = N_I$.

D. Inelastic scattering processes

In a fully rigorous solution of the BTE, all relevant scattering processes, including inelastic phonon scattering, would be included from the start. Moreover, given the dependence of charged impurity scattering on electron density, assumptions of non-degeneracy and parabolic bands should be dropped and the Fermi level calculated. However, this would greatly increase our work load and distract from the central message of the current work. This is to calculate the alloy scattering rate due to substitutional carbon and highlight both the effect of this and the possible effect of charged interstitials on the mobility. Therefore additional scattering processes are only incorporated in an empirical manner by inferring an effective relaxation time from the measured mobility of pure Si and adding this into our numerical calculations (see Sec. IV B for details).

III. THE FIRST-PRINCIPLES APPROACH

The approach to alloy scattering used here is based on first-principles calculations via density functional theory (DFT). The first step is to obtain the ground state (GS) densities for both an unperturbed system (i.e., a perfect lattice) and a perturbed system with an impurity atom via self-consistent calculations. For the former, we construct primitive two-atom cells whilst for the latter, we build large supercells. Having obtained the GS densities, we then proceed with non-self-consistent eigenvalue calculations for the conduction band states. These are then used to construct the scattering matrix elements as described in more detail in the next section.

It is well known that the DFT band structure does not necessarily reproduce the correct quasiparticle band structure that is relevant for carrier dynamics. Nevertheless, the largest error typically occurs in the band gap, rather than in the conduction or valence band dispersions. For Si and Ge, the DFT conduction-band dispersions and pressure dependence of the band gap, are generally in good agreement with experiment.^{21,22} In SiGe, the conduction-band deformation potentials and alloy composition dependence have been shown to be in excellent agreement with experiment.^{10,11} Indeed, this is the basis for using the DFT approach to calculate the carrier scattering, where it is the difference between the perturbed and unperturbed band states and energies that we are concerned with.

The self-consistent GS calculations and subsequent eigenvalue calculations were carried out using the ABINIT package.²³ Pure Si primitive cells and Si($N-1$)C(1) supercells were constructed using Troullier-Martins pseudopotentials²⁴ with the local density approximation (LDA) for the exchange-correlation functional. An energy cutoff of 40 Ha was used based on the convergence of eight-atom supercells with a single C atom. Calculations with and without ionic relaxation were performed, using modified Broyden-Fletcher-Goldfarb-Shanno minimization²⁵⁻²⁷ for the former, which takes into account both the total energy as well as the energy gradients.²⁸ For the Si($N-1$)C(1) systems, we constructed fcc 54-atom, cubic 64-atom, and cuboid 128-atom supercells (two cubic 64-atom cells stuck together).

A. The scattering matrix elements

We shall denote the eigenvalues and eigenvectors of the unperturbed system by ϵ_i^0 and $|\phi_i^0\rangle$, respectively, whilst those of the perturbed system will be denoted by ϵ_i and $|\phi_i\rangle$.

The perturbed states may be written as an expansion in the $|\phi_i^0\rangle$

$$|\phi_j\rangle = \sum_i \alpha_{ij} |\phi_i^0\rangle, \quad (17)$$

so we have

$$\alpha_{ij} = \langle \phi_i^0 | \phi_j \rangle. \quad (18)$$

The Hamiltonian of the perturbed system may then be represented in terms of the unperturbed eigenstates $|\phi_i^0\rangle$ and written in matrix form as

$$\mathbf{H}\alpha = \alpha\mathbf{E}, \quad (19)$$

where the elements of \mathbf{H} are given in terms of the unperturbed eigenvalues ϵ_i^0 and the perturbing potential ΔV as

$$H_{ij} = \frac{\delta_{ij}}{2} (\epsilon_i^0 + \epsilon_j^0) + V_{ij}, \quad (20)$$

where the $V_{ij} = \langle \phi_i^0 | \Delta V | \phi_j^0 \rangle$ are the scattering matrix elements.

The columns of α are the eigenvectors of the perturbed system expanded in terms of the $|\phi_i^0\rangle$ as in Eqs. (17) and (18), whilst \mathbf{E} is a diagonal matrix containing the perturbed eigenvalues ϵ_i . Hence the individual elements of H are given by

$$H_{ij} = \sum_k \alpha_{ik} \epsilon_k \alpha_{kj}^{-1}, \quad (21)$$

and the scattering matrix elements by

$$V_{ij} = H_{ij} - \frac{\delta_{ij}}{2} (\epsilon_i^0 + \epsilon_j^0), \quad (22)$$

where α_{kj}^{-1} implies the kj element of α^{-1} .

Note that the diagonal elements of V_{ij} involve both the perturbed and the unperturbed eigenvalues ϵ_i and ϵ_i^0 . However, since these both involve an arbitrary constant due to arbitrary zero of the periodic pseudopotentials, the difference in these energies cannot be known without some way of fixing a common zero of potential for both systems. On the other hand, the off-diagonal elements of V_{ij} only involve the perturbed energy eigenvalues. Given these elements in the form of Eq. (22), it is easy to show that the diagonal elements are insensitive to any constant shift in the energy eigenvalues.

In the case of having complete sets of perturbed and unperturbed wave functions $|\phi_i\rangle$ and $|\phi_i^0\rangle$, we may write Eq. (21) in the form

$$H_{ij} = \sum_k \langle \phi_i^0 | \phi_k \rangle \epsilon_k \langle \phi_k | \phi_j^0 \rangle. \quad (23)$$

For complete sets, the diagonal elements of H_{ij} , as given by Eq. (23), also have the same insensitivity to constant shifts in the energy eigenvalues. In practice, however, we will always be working with finite sets of eigenstates. Moreover, as the size of the system is allowed to increase to infinity, we require that $|\phi_i\rangle \rightarrow |\phi_i^0\rangle$ far from the impurity—a condition not necessarily met in the construction of a finite supercell. In this case, the elements V_{ij} represent the first Born approximation to the true scattering matrix as discussed in Ref. 10. It then becomes profitable to limit the summation in Eq. (23) by design to eliminate the contributions from the perturbed states with very different energies from those of the unperturbed states. As one restricts the energy range on the summation of perturbed states, one tends toward the result of infinite-order perturbation theory.

B. Bloch representation

Equation (22) gives a generalized expression for the scattering matrix elements V_{ij} in terms of perturbed and unperturbed eigenstates and their eigenvalues. We now wish to specialize to the case where the $|\phi_i\rangle$ are states of a supercell and the $|\phi_i^0\rangle$ are the Bloch states of the unperturbed system. In the latter case, the Bloch states are labeled by wave vector \mathbf{k} and band index n . A Bloch wave function may then be written as a plane wave expansion over the reciprocal lattice vectors \mathbf{G} of the primitive cell,

$$\phi_{n,\mathbf{k}}^0(\mathbf{r}) = V_C^{-1/2} \sum_{\mathbf{G}} C_{n,\mathbf{k}+\mathbf{G}} e^{i(\mathbf{k}+\mathbf{G})\cdot\mathbf{r}}, \quad (24)$$

where the plane-wave coefficients are normalized such that

$$\sum_{\mathbf{G}} |C_{n,\mathbf{k}+\mathbf{G}}|^2 = 1. \quad (25)$$

The wave functions of a supercell may be expanded analogously except that the summation will be over the reciprocal lattice vectors \mathbf{g} of the supercell,

$$\phi_{m,\mathbf{k}}(\mathbf{r}) = V_C^{-1/2} \sum_{\mathbf{g}} C_{m,\mathbf{k}+\mathbf{g}}^S e^{i(\mathbf{k}+\mathbf{g})\cdot\mathbf{r}}. \quad (26)$$

Here, however, the \mathbf{k} appearing in Eq. (26) is only uniquely defined within the much smaller supercell Brillouin zone (SBZ). Wave vectors beyond this that still lie within the primitive Brillouin zone (PBZ) may be mapped to a \mathbf{k} point within the SBZ via a \mathbf{g} vector. The eigenvalue of this $\mathbf{k} + \mathbf{g}$ point is then folded back into the SBZ as a supercell band state at \mathbf{k} . Hence, for definiteness, we may restrict \mathbf{k} to be within the SBZ and label the wave vector of any given Bloch state by $\mathbf{k} + \mathbf{g}_0$, where \mathbf{g}_0 is a \mathbf{g} vector lying within the PBZ. Allowing i and j to be compound indices running over n and $\mathbf{k} + \mathbf{g}_0$, the required scattering matrix elements may now be written as

$$V_{ij} = \langle \phi_{n', \mathbf{k} + \mathbf{g}'_0}^0 | \Delta V | \phi_{n, \mathbf{k} + \mathbf{g}_0}^0 \rangle. \quad (27)$$

The calculation of this quantity via Eq. (22) requires evaluation of the projections α_{ik} , where k is a compound index running over supercell band indices m and \mathbf{k} points within the SBZ:

$$\alpha_{ik} = \langle \phi_{n, \mathbf{k} + \mathbf{g}'_0}^0 | \phi_{m, \mathbf{k}} \rangle. \quad (28)$$

Now, the set of all supercell reciprocal lattice vectors \mathbf{g} will contain the \mathbf{G} as well as vectors $\mathbf{g}_0 + \mathbf{G}$. Hence, the summation over \mathbf{g} may be written

$$\sum_{\mathbf{g}} = \sum_{\mathbf{G}, \mathbf{g}_0}. \quad (29)$$

The inner product of Eq. (28) is then

$$\begin{aligned} \langle \phi_{n, \mathbf{k} + \mathbf{g}'_0}^0 | \phi_{m, \mathbf{k}} \rangle &= \sum_{\mathbf{G}', \mathbf{G}, \mathbf{g}_0} C_{n, \mathbf{k}' + \mathbf{g}'_0 + \mathbf{G}'}^* C_{m, \mathbf{k} + \mathbf{g}_0 + \mathbf{G}}^S \\ &\quad \times \delta_{\mathbf{k}' + \mathbf{g}'_0 + \mathbf{G}', \mathbf{k} + \mathbf{g}_0 + \mathbf{G}}. \end{aligned} \quad (30)$$

Since \mathbf{g}_0 lies within the PBZ, it may never be a \mathbf{G} vector. Similarly, since we have restricted \mathbf{k} to lie within the SBZ, it will never be a \mathbf{g}_0 vector. Hence the Kronecker δ in Eq. (30) may be decomposed into

$$\delta_{\mathbf{k}' + \mathbf{g}'_0 + \mathbf{G}', \mathbf{k} + \mathbf{g}_0 + \mathbf{G}} = \delta_{\mathbf{k}' \mathbf{k}} \delta_{\mathbf{g}'_0 \mathbf{g}_0} \delta_{\mathbf{G}' \mathbf{G}} \quad (31)$$

and Eq. (30) becomes

$$\langle \phi_{n, \mathbf{k} + \mathbf{g}'_0}^0 | \phi_{m, \mathbf{k}} \rangle = \sum_{\mathbf{G}} C_{n, \mathbf{k} + \mathbf{g}_0 + \mathbf{G}}^* C_{m, \mathbf{k} + \mathbf{g}_0 + \mathbf{G}}^S. \quad (32)$$

Note that this summation involves only the $\mathbf{g}_0 + \mathbf{G}$ components of the supercell wave function expansion.

Calculation of the projection in Eq. (32) requires (i) having the plane-wave representations of the Bloch state with wave vector $\mathbf{k}' = \mathbf{k} + \mathbf{g}_0$ and supercell state with wave vector \mathbf{k} and (ii) a method of selecting those \mathbf{g} vectors in the supercell expansion corresponding to \mathbf{g}_0 . The first requirement is provided for via the non-self-consistent calculations of the conduction band states based on the GS density using a plane-wave code such as ABINIT. The second may be achieved by converting the \mathbf{g} vectors to primitive cell \mathbf{G} coordinates via a matrix transformation. The integral parts are then subtracted and the fractional parts transformed back to \mathbf{g} -coordinates via the inverse transformation. This is essentially the generalization of modular arithmetic to matrix multiplication, so that we might write symbolically $\mathbf{g}_0 = \mathbf{g}(\text{mod}\mathbf{G})$.

C. Mixing of originally degenerate states

In Refs. 10 and 11, scattering was considered between states that were degenerate in the unperturbed system and that folded back to the Γ point in the SBZ. In this case, the \mathbf{k} point associated with the supercell states is $\mathbf{k} = 0$ and the perturbed Hamiltonian may be written

$$H_{\mathbf{g}'_0 \mathbf{g}_0} = \sum_m \langle \phi_{\mathbf{g}'_0}^0 | \phi_m \rangle \epsilon_m \langle \phi_m | \phi_{\mathbf{g}_0}^0 \rangle, \quad (33)$$

where the summation is over the bands at the Γ point.

As a particular example, the \mathbf{g}_0 may map to points along the Δ line, so that the scattering matrix elements obtained from Eq. (33) are for intravalley ($\mathbf{g}'_0 = \mathbf{g}_0$), f -type intervalley (\mathbf{g}'_0 orthogonal to \mathbf{g}_0) and g -type ($\mathbf{g}'_0 = -\mathbf{g}_0$) intervalley scatterings. These may be denoted by V_Δ , V_f , and V_g , respectively. Rather than calculating these elements directly from an expression of the form of Eq. (22), a reduced 6×6 matrix defined by Eq. (33) in terms of the six possible \mathbf{g}'_0 vectors may be diagonalized, yielding one, two, and threefold degenerate eigenvalues ϵ_1 , ϵ_2 , and ϵ_3 , respectively, which may only be known with respect to an arbitrary additive constant δV , as discussed in the next section. The V_i may then be expressed in terms of the ϵ_i according to¹¹

$$V_\Delta = \frac{1}{6}(\epsilon_1 + 2\epsilon_2 + 3\epsilon_3) - \delta V, \quad (34)$$

$$V_g = \frac{1}{6}(\epsilon_1 + 2\epsilon_2 - 3\epsilon_3), \quad (35)$$

and

$$V_f = \frac{1}{6}(\epsilon_1 - \epsilon_2). \quad (36)$$

One advantage of this approach is that it automatically takes care of any arbitrary mixing of degenerate states. It may be shown that the diagonalization of a matrix H_{ij} for which the unperturbed states are degenerate is insensitive to the way in which the states are mixed. This is not the case for the matrix elements obtained from the more general expression in Eq. (22) using either Eq. (21) or Eq. (23).

D. q-point interpolation

A remaining problem with the application of Eq. (34) for intravalley scattering arises from the arbitrary zero of energy for a periodic potential. This means that the relative shift δV between the potentials in the perturbed and unperturbed systems will be undetermined. Moreover, we see from Eq. (10) that the error in the calculation of the alloy intravalley scattering parameter is equal to $N\delta V$, so that for the above prescription to be useful, we would need some way of finding δV such that it gets smaller with supercell size at least as fast as $1/N$.

In Refs. 10, 11 and 29, a method of averaging the difference in the local potentials of the perturbed and unperturbed systems was employed. In that work and a previous application of the method to C in Si,³⁰ the matrix elements were based on a supercell representation, i.e., the unperturbed states were calculated for supercells without any scattering perturbation. The accuracy of this approach then depends on the precision with which the potentials may be determined.

An important factor affecting the accuracy of DFT calculations is the cutoff energy ϵ_{cut} used to determine the number

of plane-waves used in the construction of the GS density. In the present work, the cutoff energy is kept fixed for all calculations, so this will not have any supercell size dependent effect on the determination of the potential. However, ϵ_{cut} does determine the fast Fourier transform (FFT) grid on which periodic functions such as the potential are defined. The real space FFT grid points are given in terms of the reduced direct space lattice vectors, which will be different for different supercell geometries. Hence, direct point-to-point comparison between potentials is only possible for cells with the same FFT grids. Otherwise, some interpolation method must be used and, as we shall see, this can introduce unacceptable errors.

If the unperturbed and perturbed systems are both constructed using supercells with the same geometry, then the error in determining the difference between the potentials will decrease with supercell size. This is because the relative contribution of the perturbation becomes smaller and the potentials far from the impurity site will tend more closely to one another. Since supercells with the same size, geometry, and cutoff energy will use the same FFT grid, a direct comparison may be made such that the error in the alloy scattering parameter will be canceled by the increased accuracy with which the difference in potentials may be determined.

The comparison of commensurate supercells will still be subject to a further problem. The supercell states, subsequently calculated non-self-consistently using the GS density, will generally be arbitrary superpositions of Bloch states. Hence the scattering matrix constructed from them will also be a (generally unknown) superposition of the required matrix between Bloch states. However, trying to calculate the difference between the potentials in the primitive cell and perturbed supercell leads to the immediate problem that the potentials for the two systems are usually defined on incommensurate FFT grids. Thus the accuracy with which the difference between the potentials can be known will be limited by the accuracy of the numerical interpolation used, as opposed to finding the difference at the same FFT grid points without the need for interpolation. Since the FFT grids are fixed by the cutoff energy, the error in δV cannot decrease with cell size and the error in the alloy scattering potential must increase in proportion to N .

A way of circumventing this problem is to use the more general formulation of the model and calculate off-diagonal matrix elements for nonzero scattering vectors $\mathbf{q} = \mathbf{k} - \mathbf{k}'$. In this case, the eigenvalues of the unperturbed system disappear from the calculation as pointed out in Sec. III, so the difference between the arbitrary zeros of the potentials is no longer a problem. As the size of a supercell increases, the reciprocal lattice vectors, which are the allowed \mathbf{q} vectors for the system, become smaller. This then offers the possibility of interpolating the scattering matrix elements to $\mathbf{q} = 0$. The strategy employed here to overcome limitations on the computational resources needed for very large supercells is to construct long supercells that have much smaller reciprocal lattice vectors along one axis. In particular, we construct cuboid 128-atom supercells by concatenating two cubic 64-atom cells.

Possible problems with the interpolation may arise due to the arbitrary phase of a Bloch function, which may cause the relative phase between the Bloch functions involved in the alloy scattering matrix element to change discontinuously. To

deal with this problem, we monitor the behavior of the the overlap factor $I_{\mathbf{k}'\mathbf{k}}^{n'n}$, defined as the inner product of the periodic parts of the Bloch functions $\phi_{n'\mathbf{k}'}$ and $\phi_{n\mathbf{k}}$ integrated over the primitive cell. Hence, writing a Bloch function in the form $\phi_{n\mathbf{k}}^0(\mathbf{r}) = u_{n\mathbf{k}}(\mathbf{r})e^{i\mathbf{k}\cdot\mathbf{r}}$, we have [c.f. Eq. (24)]

$$\begin{aligned} I_{\mathbf{k}'\mathbf{k}}^{n'n} &= \int_{PC} u_{n'\mathbf{k}'}^*(\mathbf{r})u_{n\mathbf{k}}(\mathbf{r})d^3\mathbf{r}, \\ &= \sum_{\mathbf{G}} C_{n',\mathbf{k}'+\mathbf{G}}^* C_{n,\mathbf{k}+\mathbf{G}}. \end{aligned} \quad (37)$$

$I_{\mathbf{k}'\mathbf{k}}^{n'n}$ therefore contains information about the relative phase between the Bloch functions.

Since the scattering matrix of Eq. (27) is constructed entirely from Bloch functions and the real energy eigenvalues of the supercell, if $I_{\mathbf{k}'\mathbf{k}}^{n'n}$ varies smoothly with $\mathbf{q} = \mathbf{k} - \mathbf{k}'$, we may attribute any sudden change in phase (in practice, sign reversal) to the effect of the scattering potential. On the other hand, in certain cases, such as when the scattering vector \mathbf{q} translates the initial \mathbf{k} point through the Γ point or into the adjacent BZ, the sign of $I_{\mathbf{k}'\mathbf{k}}^{n'n}$ may reverse. In this case, the sign reversal is a feature of the Bloch functions. Hence, to counter any anomalous artifacts of the matrix diagonalizer used to calculate the Bloch functions, we impose any sudden change in the phase of $I_{\mathbf{k}'\mathbf{k}}^{n'n}$ onto the scattering matrix.

IV. RESULTS

A. Alloy scattering parameters

In Figs. 1 and 2, we show the results of calculations for scattering by substitutional C in Si for unrelaxed and relaxed structures using Eq. (33) for the reduced 6×6 matrix method

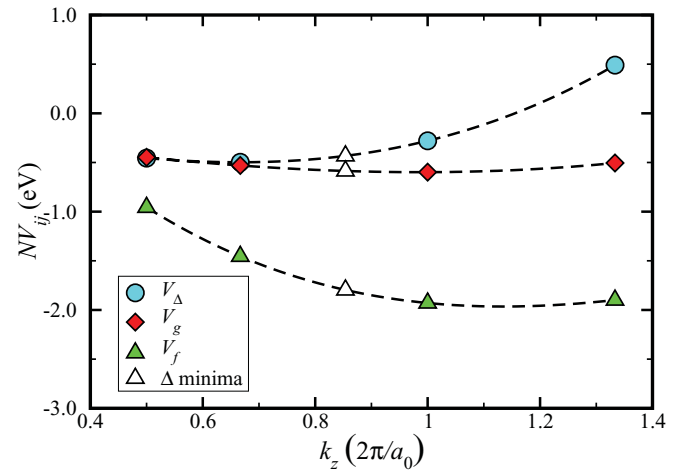


FIG. 1. (Color online) Calculations for the scattering parameters in unrelaxed $\text{Si}_{1-x}\text{C}_x$ using the 6×6 matrix method of Eq. (33). Points at $k_z = 1/2$ and $k_z = 1$ were obtained from a cubic 64-atom supercell. For the points at $k_z = 2/3$ and $k_z = 4/3$ an fcc 54-atom supercell was used. The criterion used for the number of supercell states to include in the scattering matrix was based on the absolute difference of the perturbed supercell energies ϵ and the originally sixfold degenerate unperturbed Bloch-states energies ϵ_0 being less than or equal to 4 eV. The white triangles mark the polynomial interpolation to the Δ valley minimum, with values of -0.4 , -0.6 , and -1.8 eV for intravalley, g -type, and f -type scatterings, respectively.

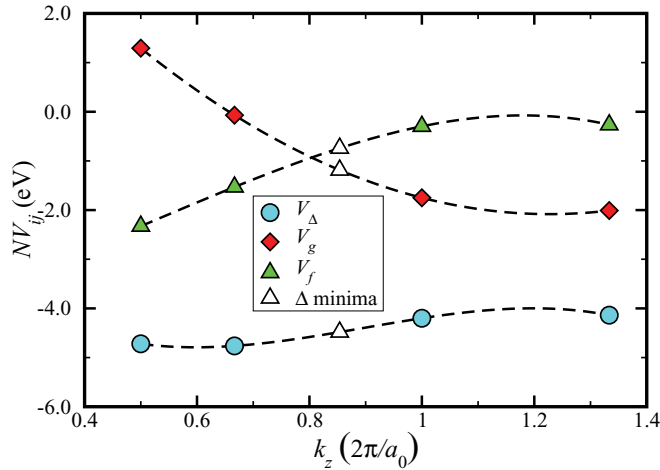


FIG. 2. (Color online) Calculations for the scattering parameters in relaxed $\text{Si}_{1-x}\text{C}_x$ using the 6×6 matrix method of Eq. (33). The same comments given in the caption to Fig. 1 apply here. The polynomial interpolations to the Δ -valley minimum yield values of -4.5 , -1.2 , and -0.7 eV for intravalley, g -type, and f -type scatterings, respectively.

for originally degenerate eigenvalues that fold back to the Γ point in the constructed supercell. The supercells used for these calculations were an FCC 54-atom cell and a cubic 64-atom cell. In these cells, points along the Δ line are mapped back to $\mathbf{k} = 0$ via reciprocal lattice vector translations. In particular, as a fraction of the distance along the Δ line to the X point, the 54-atom cell gives us points at $2/3$ and $4/3$, whilst the 64-atom cell gives us points at $1/2$ and 1 . These points are then interpolated to the Δ -valley minimum shown as white triangles in the graphs.

The choice of which perturbed supercell states in Eq. (21) to use for the construction of the scattering matrix H_{ij} is based on the difference in energy between the perturbed and unperturbed states. Specifically, we only include states with energies within 4 eV of the unperturbed eigenvalues. The rationale behind this is that we wish the wave-function states in the scattering matrix element to match that of a specific unperturbed Bloch state of the pure Si system far from the impurity, while matching that of an eigenstate with the defect present near the C atom, and hence to reproduce the distorted wave approximation (or the scattering amplitude in the Lippmann-Schwinger equation) more closely.¹⁰

The fact that the calculated values of the alloy scattering potential do not diverge with cell size indicates that the splittings of the originally degenerate eigenvalues reduce as $1/N$ [c.f. Eq. (10)]. Although we have only shown results in this paper for 54-atom, 64-atom, and 128-atom cuboid cells, calculations have also been carried out for a 16-atom, 32-atom, and 128-atom fcc cells bearing out the same conclusion. This indicates that the substitutional carbon does not produce a localized state, since if it did, we would see the emergence of a fixed energy state that varied little with \mathbf{k} vector.

In the case of intravalley scattering, δV was estimated by a twofold process. First, SCF calculations are carried out for commensurate supercells of pure Si and Si perturbed by a substitutional carbon atom. The potentials at fixed positions (under ionic relaxation) furthest from the substitutional site

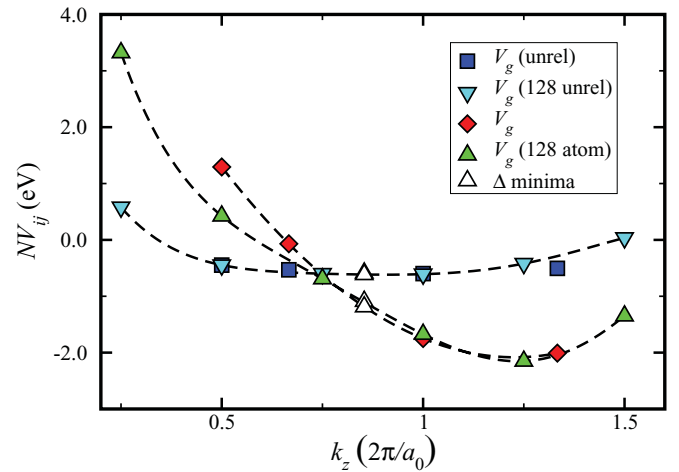


FIG. 3. (Color online) Comparison of the calculations for g -type scattering in $\text{Si}_{1-x}\text{C}_x$ using (i) the 6×6 matrix method and (ii) from the elements of the unreduced scattering matrix of a cuboid 128-atom supercell. The data points for method (i) are the blue squares (unrelaxed structure) and red diamonds (relaxed structure), also plotted in Figs. 1 and 2, respectively. For method (ii), the down-pointing cyan triangles are for the unrelaxed structure and the upright green triangles are for the relaxed structure. Interpolating to the Δ -valley minimum for the second set of calculations gives values of -0.6 and -1.1 eV for the unrelaxed and relaxed structures, respectively.

are found and the difference taken. We may denote these values by $V_{\text{Si}(N)}$ and $V_{\text{Si}(N-1)\text{C}(1)}$ for the pure and perturbed systems, respectively, and define $\delta V_{\text{SC}} = V_{\text{Si}(N-1)\text{C}(1)} - V_{\text{Si}(N)}$. Next, the difference between the eigenvalues of the pure Si supercell $\epsilon_{\text{Si}(N)}$ and the primitive cell $\epsilon_{\text{Si}(2)}$ at the appropriate \mathbf{k} point is found $\delta \epsilon_{\text{Si}} = \epsilon_{\text{Si}(N)} - \epsilon_{\text{Si}(2)}$. These are then both incorporated into the total difference $\delta V = \delta V_{\text{SC}} + \delta \epsilon_{\text{Si}}$. This is a similar approach to that used previously for SiGe.¹⁰

As a comparison of the methods using the 6×6 matrix and \mathbf{q} -point interpolation, Fig. 3 shows the results for g -type scattering calculated using the former method and the more general scattering matrix for a cuboid 128-atom supercell. The reciprocal lattice vectors of the 128-atom cell along its long axis (in real space) give points along the Δ line separated by $1/4$ as a fraction of the distance to the X point.

The same energy criterion is chosen in both cases to compare like with like, although with \mathbf{q} -point interpolation there are two unperturbed energy values for each matrix element to consider. Here, the criterion is taken to be that the supercell eigenvalues are within 4 eV of either of the unperturbed energies.

Figure 4 shows the calculation for intravalley scattering in the 128-atom cell with the \mathbf{q} relative to the Δ -valley minimum. Here the possible discrepancies between the methods due to the accuracy in determining δV show up in the unrelaxed case. We find here that \mathbf{q} -point interpolation gives a value for intravalley scattering of 0.2 eV, whereas the 6×6 matrix method gives -0.4 eV (shown on the graph for comparison). If this is attributed to the error in δV , then for the size of the supercells used it would correspond to an error of ~ 0.01 eV. To put this figure into perspective, the interpolation utility that comes bundled with the ABINIT package gives an error of

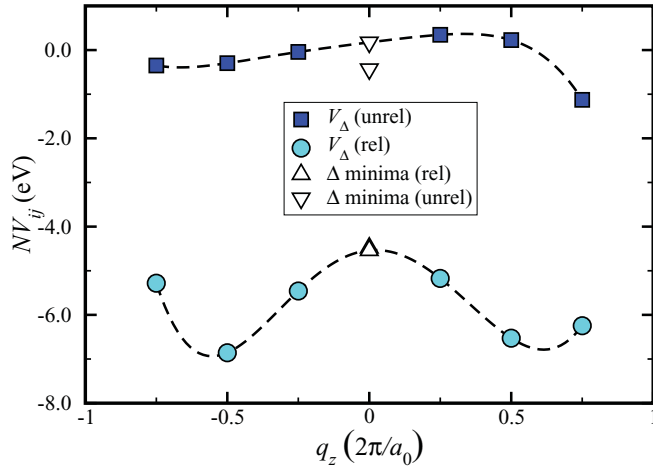


FIG. 4. (Color online) Calculations for intravalley scattering in $\text{Si}_{1-x}\text{C}_x$ using the elements of the unreduced scattering matrix for a cuboid 128-atom supercell. Here, the matrix elements are for the \mathbf{q} -point scattering vector from the Δ -valley minimum. Hence, the interpolation is to $\mathbf{q} = 0$, giving values of 0.2 and -4.5 eV for the unrelaxed and relaxed structures, respectively. Also shown for comparison are the values interpolated to the Δ -valley minimum calculated via the 6×6 matrix method, -0.4 and -4.5 eV for the unrelaxed and relaxed structures, respectively (c.f Figs. 1 and 2).

~ 0.03 eV between the potentials at the basis atom sites in the Si primitive cell. The results for the calculated alloy scattering potentials are summarized in Table I.

B. Calculated mobilities

Figure 5 shows a comparison of experimental mobilities by Osten *et al.*⁴ and calculated mobilities using Eq. (4) with the results of the last section for the alloy scattering matrix elements in relaxed $\text{Si}_{1-x}\text{C}_x$. The results of Osten *et al.* show a degradation of the mobility, even for lower C concentrations. These researchers grew $0.2 \mu\text{m}$ thick $\text{Si}_{1-x}\text{C}_x$ layers with a nominal antimony doping of $1 \times 10^{17} \text{cm}^{-3}$. Note that as well as the suppression of the mobility at higher temperatures following a $T^{-1/2}$ dependence, consistent with alloy scattering, there appears to be additional limiting processes at lower temperatures following a $T^{3/2}$ dependency, characteristic of ionized impurity scattering. Indeed, Osten *et al.* argue for the formation of electrically active defects due to interstitial carbon complexes suppressing the mobility.

In the theoretical calculations, the scattering processes in pure Si have been incorporated by fitting the experimental mobility to combined scattering rates with $\epsilon^{-3/2}$, $\epsilon^{1/2}$, and

TABLE I. Calculated alloy scattering parameters [see Eq. (10)] for substitutional C in Si. All values are in eV.

Method		Unrelaxed	Relaxed
6×6 matrix	Intravalley	-0.4	-4.5
	f type	-1.8	-0.7
	g type	-0.6	-1.2
\mathbf{q} -point interpolation	Intravalley	0.2	-4.5
	g type	-0.6	-1.1

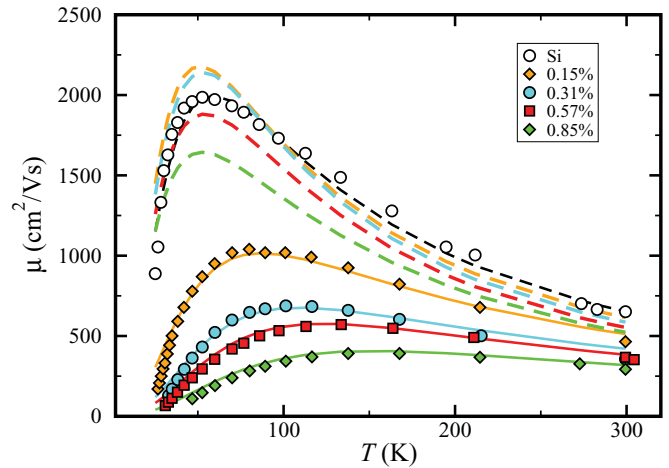


FIG. 5. (Color online) Experimental Hall mobilities by Osten *et al.* (symbols) and calculated mobilities for the same C doping. The scattering processes in pure Si have been incorporated by fitting the experimental mobility to combined scattering rates with $\epsilon^{-3/2}$, $\epsilon^{1/2}$, and $\epsilon^{3/2}$ dependencies, including a screening factor on the $\epsilon^{-3/2}$ rate (representing ionized impurity scattering). These are then combined with the rates for alloy scattering due to substitutional carbon (dashed lines) and both alloy scattering and additional charged impurity scattering due to electrically active defects (solid lines). At the high-temperature side (right of graph), the lines decrease in mobility with increasing x . The highest dashed line is the fit to the pure Si mobility.

$\epsilon^{3/2}$ dependencies. The process varying as $\epsilon^{-3/2}$ is taken to be ionized impurity scattering and multiplied by the screening factor given by Eq. (14) using the experimentally measured carrier concentration to determine the reciprocal screening length q_0 . The highest dashed line on the high-temperature side of Fig. 5 shows this fit.

Alloy scattering due to substitutional C is then added in (the dashed lines in Fig. 5). For the energy splitting, we used $\Delta\epsilon = 5.6x$ eV from Ref. 31, where this dependency was fitted to tight-binding band-structure calculations. This value was confirmed by our own DFT calculations for strained Si, which had the concomitant result of confirming that there was a negligible change in the effective masses.

We note that, in the absence of any other scattering mechanisms, the addition of C initially increases the mobility at low temperature for the lower x concentrations (0.15% and 0.31%). However, it is clear that alloy scattering alone does not explain the observed degradation of the mobility in the samples.

To model the experimental results, we assume that the additional scattering is due to ionized impurity scattering caused by electrically active defects. It is known that substitutional C reacts with interstitial Si, being “kicked out” to form the highly mobile C interstitial C_i .³² Although these defects may be electrically active, they tend to migrate until they are captured by another substitutional C atom to form the immobile C_iC_s complex.³³ These interstitial defects are known to have a bistable configuration in which they may be either positively or negatively charged.⁸ Further C complexes are also possible depending on the environmental conditions.³³ The actual number of stable interstitial sites will be determined by the solid solubility limit ($\sim 10^{17} \text{cm}^{-3}$).⁴

TABLE II. Concentrations of charged interstitials N_I used to model the additional charged impurity scattering.

x (%)	N_I (cm^{-3})
0.15	3.8×10^{16}
0.31	1.2×10^{17}
0.57	1.6×10^{17}
0.85	3.7×10^{17}

Without *a priori* knowledge of the concentrations of electrically active interstitials N_I , we use Eq. (13) to model the additional charged impurity scattering, fitting the number of scattering centres to the experimental results. The calculations are shown in Fig. 5 as the solid lines passing (very closely) through the associated data points. The charged interstitial concentrations used are given in Table II.

We note that although the experimental results of Eberl *et al.*⁵ do not show the same degradation in mobility, our results for alloy scattering alone are not inconsistent with the measured data. In particular, the peak value of the mobility measured by Eberl *et al.* for $\text{Si}_{1-x}\text{C}_x$ with $x = 0.4\%$ occurs at $T \approx 45$ K with a value of $\sim 6750 \text{ cm}^2(\text{Vs})^{-1}$. At the same temperature, the calculated alloy scattering-limited mobility (i.e., the mobility calculated via Eqs. (4)–(6) in the absence of all other scattering process) is $9900 \text{ cm}^2(\text{Vs})^{-1}$ and remains greater than the measured mobility at all other temperatures. One difference between the samples studied by Eberl *et al.* and Osten *et al.* is that the former used phosphorus at a concentration of $\sim 3 \times 10^{17} \text{ cm}^{-3}$ as the *n*-type donor, whereas the latter used antimony doped at $\sim 1 \times 10^{17} \text{ cm}^{-3}$. We tentatively suggest that P may then passivate the charged C interstitials in some way, or react with the C complexes to form mobile interstitials that then diffuse out of the $\text{Si}_{1-x}\text{C}_x$ layers. This would explain the absence of additional charged impurity scattering in the P-doped samples.

A possible shortcoming of the mobility calculations presented here is that the contribution due to phonon-scattering is only implicitly incorporated via fitting of unstrained Si. In a more rigorous approach, we should include each scattering process explicitly, including the effect of the splitting of the Δ valleys due to the biaxial strain.

V. CONCLUSIONS

We have investigated alloy scattering due to substitutional carbon in silicon via the application of a first-principles approach. A more effective way of obtaining the intravalley

scattering rate has been introduced via interpolation to $\mathbf{q} = 0$ of the scattering matrix elements as a function of \mathbf{q} . However, this method is less useful than that used in Refs. 10 and 11 for the calculation of *f*-type scattering (since the scattering to the Δ -valley minimum in an orthogonal valley generally requires interpolation over a plane in \mathbf{k} space) and does not automatically cope with degenerate states as the 6×6 matrix method does. The results of both methods are compared in Figs. 3 and 4, showing good agreement for *g*-type scattering.

This work has led to a number of conclusions. Firstly, both concomitant band-structure calculations and the non-divergence of the alloy scattering potential with increasing cell size indicated that substitutional carbon does not form a localized state. This is important for two reasons. Firstly, if a localized state is being formed, we might reasonably expect this to produce very strong scattering in analogy with N in III-V semiconductors.¹² Secondly, if, as in the case of dilute nitrides, the localized state was resonant with the conduction band then our present first-principles model would not be directly applicable.

However, the alloy scattering potential is still very strong, certainly in comparison with values of ~ 0.6 eV found in SiGe systems.¹⁰ In relaxed $\text{Si}_{1-x}\text{C}_x$ the strongest scattering process is intravalley scattering, with a matrix element of -4.5 eV, followed by *g*-type intervalley scattering with -1.1 to -1.2 eV. The weakest process is *f*-type intervalley scattering at -0.7 eV. We note that ionic relaxation has a large effect on the intravalley scattering.

The validity of the scattering model for elemental alloys was previously demonstrated in Refs. 10 and 11. Calculations for the alloy scattering-limited mobility in biaxially strained $\text{Si}_{1-x}\text{C}_x$ show that scattering by substitutional C cannot account alone for the degradation in the mobility observed by Osten *et al.* Assuming that some proportion of interstitial C complexes form electrically active scattering sites and modeling this via the Brooks-Herring model for charged impurity scattering, we have shown that the observed mobilities can be fully accounted for. Moreover, the concentrations of additional electrically active defects found from this fitting are consistent with solid solubility limits for C interstitials and show a monotonic increase with C doping. These findings suggest that the effect of interstitial C on the transport properties of $\text{Si}_{1-x}\text{C}_x$ is much greater than that due to substitutional C. This provides the motivation for a deeper study of the effect on transport of interstitial complexes in the presence of P or Sb.

ACKNOWLEDGMENT

This work was supported by Science Foundation Ireland.

*martin.vaughan@tyndall.ie

¹S. C. Jain, H. J. Osten, B. Dietrich, and H. Rucker, *Semicond. Sci. Tech.* **10**, 1289 (1995).

²H. J. Osten, H. Rucker, J. P. Liu, and B. Heinemann, *Microelectron. Eng.* **56**, 209 (2001).

³C. F. Tan, E. F. Chor, J. Liu, H. Lee, E. Quek, and L. Chan, *Appl. Phys. Lett.* **83**, 4169 (2003).

⁴H. J. Osten and P. Gaworzewski, *J. Appl. Phys.* **82**, 4977 (1997).

⁵K. Eberl, K. Brunner, and W. Winter, *Thin Solid Films* **294**, 98 (1997).

⁶G. D. Watkins and K. L. Brower, *Phys. Rev. Lett.* **36**, 1329 (1976).

⁷L. W. Song and G. D. Watkins, *Phys. Rev. B* **42**, 5759 (1990).

⁸L. W. Song, X. D. Zhan, B. W. Benson, and G. D. Watkins, *Phys. Rev. Lett.* **60**, 460 (1988).

- ⁹L. W. Song, X. D. Zhan, B. W. Benson, and G. D. Watkins, *Phys. Rev. B* **42**, 5765 (1990).
- ¹⁰F. Murphy-Armando and S. Fahy, *Phys. Rev. Lett.* **97**, 096606 (2006).
- ¹¹F. Murphy-Armando and S. Fahy, *Phys. Rev. B* **78**, 035202 (2008).
- ¹²W. Shan, W. Walukiewicz, J. W. Ager III, E. E. Haller, J. F. Geisz, D. J. Friedman, J. M. Olson, and S. R. Kurtz, *Phys. Rev. Lett.* **82**, 1221 (1999).
- ¹³S. Fahy, A. Lindsay, H. Ouerdane, and E. P. O'Reilly, *Phys. Rev. B* **74**, 035203 (2006).
- ¹⁴B. K. Ridley, *Quantum Processes in Semiconductors*, 4th ed. (Clarendon Press, Oxford, 1999).
- ¹⁵P. A. Flinn, *Phys. Rev.* **104**, 350 (1956).
- ¹⁶L. Nordheim, *Ann. Phys.* **9**, 607 (1931).
- ¹⁷G. L. Hall, *Phys. Rev.* **116**, 604 (1959).
- ¹⁸A. E. Asch and G. L. Hall, *Phys. Rev.* **132**, 1047 (1963).
- ¹⁹J. W. Harrison and J. R. Hauser, *Phys. Rev. B* **13**, 5347 (1976).
- ²⁰H. Brooks, *Adv. Electron. Electron Phys.* **7**, 85 (1955).
- ²¹K. J. Chang, S. Froyen, and M. L. Cohen, *Solid State Commun.* **50**, 105 (1984).
- ²²X. Zhu, S. Fahy, and S. G. Louie, *Phys. Rev. B* **39**, 7840 (1989).
- ²³X. Gonze *et al.*, *Comp. Mater. Sci.* **25**, 478 (2002).
- ²⁴N. Troullier and J. L. Martins, *Phys. Rev. B* **43**, 1993 (1991).
- ²⁵C. G. Broyden, *Math. Comput.* **21**, 368 (1967).
- ²⁶D. Goldfarb, *Math. Comput.* **24**, 23 (1970).
- ²⁷D. F. Shanno, *Math. Comput.* **24**, 647 (1970).
- ²⁸H. B. Schlegel, *J. Comput. Chem.* **3**, 214 (1982).
- ²⁹S. Joyce, F. Murphy-Armando, and S. Fahy, *Phys. Rev. B* **75**, 155201 (2007).
- ³⁰M. P. Vaughan and S. Fahy, *J. Phys.: Conf. Ser.* **242**, 012003 (2010).
- ³¹S. T. Chang and C. Y. Lin, *Jpn. J. Appl. Phys.* **44**, 2257 (2005).
- ³²J. Tersoff, *Phys. Rev. Lett.* **64**, 1757 (1990).
- ³³A. Mattoni, F. Bernardini, and L. Colombo, *Phys. Rev. B* **66**, 195214 (2002).